SECOND LAW ANALYSIS OF MHD FORCED CONVECTIVE NANOLIQUID
FLOW THROUGH A TWO-DIMENSIONAL CHANNEL

Rached MIRI , **Mohamed A. ABBASSI*** , **Mokhtar FERHI**** , **Ridha DJEBALI****

*Research Lab, Technology Energy and Innovative Materials, Faculty of Sciences, University of Gafsa, Gafsa 2112, Tunisia
**UR: Modelling Optimization and Augmented Engineering, ISLAIB, University of Jendouba, Av. de l'UMA, Jendouba 8189, Tunisia

rachedmiri111@gmail.com, abbassima@gmail.com, moktar.ferhi@gmail.com, jbelii_r@hotmail.fr

Abstract: The present study deals with fluid flow, heat transfer and entropy generation in a two-dimensional channel filled with Cu–water nanoliquid and containing a hot block. The nanoliquid flow is driven along the channel by a constant velocity and a cold temperature at the inlet, and the partially heated horizontal walls. The aim of this work is to study the influence of the most important parameters such as nanoparticle volume fraction ($0\% \leq \phi \leq 4\%$), nanoparticle diameter ($5\ nm \leq dp \leq 55\ nm$), Reynolds number ($50 \leq Re \leq 200$), Hartmann number ($0 \leq Ha \leq 90$), magnetic field inclination angle ($0 \leq \gamma \leq \pi$) and Brownian motion on the hydrodynamic and thermal characteristics and entropy generation. We used the lattice Boltzmann method (LBM: SRT-BGK model) to solve the continuity, momentum and energy equations. The obtained results show that the maximum value of the average Nusselt number is found for case (3) when the hot block is placed between the two hot walls. The minimum value is calculated for case (2) when the hot block is placed between the two insulated walls. The increase in Reynolds and Hartmann numbers enhances the heat transfer and the total entropy generation. In addition, the nanoparticle diameter increase reduces the heat transfer and the irreversibility, the impact of the magnetic field inclination angle on the heat transfer and the total entropy generation is investigated, and the Brownian motion enhances the heat transfer and the total entropy generation.

Key words: MHD, LBM, channel flow, nanoliquid, entropy generation, Brownian motion

1. INTRODUCTION

In the last few decades, simulation of flow, convective heat transfer and irreversibility in channels has attracted considerable attention due to various industrial applications, such as air conditioning systems in buildings, cooling of electronic components, compact heat exchangers and biomedical equipment. Several research studies are developed in this context using different emerging CFD methods, such as finite volume method, finite element method and lattice Boltzmann method (LBM).

Recently, the LBM based on the LB equation has been viewed as a novel alternative to discretisation methods. This technique is a powerful approach for scrutinising fluid flow and heat transfer difficulties because it is a second-order accuracy in both time and space; it is easy to code and may be used to handle the extended range of flow regimes ranging from microscopic to continuum scales. Besides, the application of the LBM technique has received continuous interest in the last decades for the simulation of classic and emerging CFD [1-2].

Since the importance of the heat transfer phenomenon and its applications in various fields, it is necessary to present a few examples of research work, interlaced by the various parameters and various boundary condition influencing the rate of heat transfer. Mishra et al. [3] studied the forced convection heat transfer from an isothermal heated cone in Bingham plastic fluids using the finite element method. They found that the heat transfer rate

exhibits a positive dependence on Reynolds and Prandtl numbers. Kim [4] used the finite element method to study the forced convection heat transfer and fluid flow between parallel plates under uniform heat flux. They concluded that the formulation for the Nusselt number has been derived based on the analytically described velocity and flow rate. Peyghambarzadeh et al. [5] studied the forced convection and sub cooled flow boiling heat transfer to pure water and n-heptane in an annular heat exchanger using experimental correlations. They concluded that although n-heptane leaves the heat exchanger warmer at similar operating conditions, it has a less heat transfer coefficient than water, and the heat transfer coefficient is a direct function of heat flux, sub cooling temperature and fluid flow rate. Araste et al. [6] performed a 2-D numerical study of hydrothermal performance of a porous sinusoidal double-layered heat sink using silver–water nanofluid in a laminar regime. They showed that the dimensionless optimum porous thicknesses are equal to 0.8, 0.8 and 0.2 for the cases when Darcy numbers are equal to 10^{-4}, 10^{-3} and 10^{-2}, respectively. The maximum performance evaluation criteria number equal to 2.12 is obtained for the case with Darcy number equal to 10^{-2}, Reynolds number equal to 40, and volume fraction of nanoparticles equal to 0.04. Farooq et al. [7] studied the 3D bioconvection flow of carreau nanofluid in the presence of thermal radiation. The results show that a higher temperature profile is observed with higher values of thermal Biot number, exponential basic sink parameter and thermal relaxation, while a decrease in temperature is observed with an increase in mixed convection. Also, they

Rached Miri, Mohamed A. Abbassi, Mokhtar Ferhi, Ridha Djebali
Second Law Analysis of MHD Forced Convective Nanoliquid Flow Through a Two-Dimensional Channel

DOI 10.2478/ama-2022-0050

found that the concentration profile shows a growing tendency with the mass concentration parameter and the concentration relaxation parameter, and the microorganism field depends directly on the Peclet number and bioconvection Lewis number. Xiong et al. [8] explained the important aspects of viscous dissipation on the magneto-cross-nanofluid flow crossed by a needle placed in a porous environment. As we know, the heat transfer of the most conventional fluids is not suitable for many actual processes due to the low thermal conductivity. Adding nanoparticles to the base fluid is a new idea for improving heat transfer in these types of fluid, named 'nanofluids'. Santra et al. [9] used the control volume approach to investigate the heat transfer enhancement due to nanofluid flow through two isothermally heated parallel plates. The obtained results show that the increase in the solid volume fraction improves the heat transfer rate. Heidary and Kermani [10] investigated the flow and heat transfer in sinusoidal wall channel crossed with the Cu–water nanofluid. They concluded that the heat transfer increases with the increasing nanoparticle volume fraction and Reynolds numbers. Minakov et al. [11] experimentally studied the forced convection of nanofluids with CuO nanoparticles in a copper tube of a length of 1 m, an outer diameter of 6 mm and an inner diameter of 4 mm. The average heat transfer coefficient increased with the mass flow rate. The concentration of nanoparticles had a significant influence on the dependency of the average heat transfer coefficient on the flow rate. Ma et al. [12] investigated the convective heat transfer of the Al2O3–water in a bent channel using the LBM. The results of this study show that the local and average Nusselt numbers increased with the increasing nanoparticle volume fraction, regardless of the Re and vertical passage ratio. Moreover, the effect of the nanofluid concentration on the increment of heat transfer was more remarkable at higher values of the Reynolds number. Simulations show that by increasing the Reynolds number or decreasing the vertical passage ratio, the local and average Nusselt numbers increase. Ramin et al. [13] analysed thermal and hydrodynamic characteristics of Al2O3/Cu–water hybrid nanofluid in a 3D sinusoidal double-layered microchannel heat sink. They found that the sinusoidal shape of the microchannel walls and addition of solid nanoparticle volume fraction (Al2O3/Cu) in the base fluid have a positive effect on increasing heat transfer, and the value of Nusselt number increases about 23%, 22%, 19% and 13% for Re = 50, 300, 700 and 1,200, with a nanoparticle volume fraction of 2%. Also, the results show that adding nanoparticles to the traditional fluid elevates temperature and dynamic viscosity of the base fluid. Mohebbi et al. [14] studied the forced convection heat transfer from surface mounted blocks attached to the bottom wall of a horizontal channel with the Cu–water nanofluid using the second-order LBM. The results show that heat transfer in channels can be enhanced by using the block on the walls and adding nanoparticles. There is a maximum value of 39.04% increase in the average heat transfer coefficient for the all examined cases compared to the base fluid. Lotfi et al. [15] studied the forced convective heat transfer of Al2O3–water in horizontal tubes using the two-phase Eulerian model. The results show that the rate of thermal enhancement decreases with the increase of nanoparticle volume concentration. Mahian et al. [16] studied the advantages of using nanofluids. The results show that the addition of nanoparticles and the use of smaller size nanoparticles lead to higher heat transfer improvement rates. Almohammadi et al. [17] experimentally investigated the thermal conductivity of Al2O3–water in the laminar flow regime in a circular tube. The results emphasise that the average heat transfer coefficient is improved by 27% and 20% for a vol-

ume concentration of Al2O3 equal to 1% and 0.5%, respectively, compared to the base fluid. Heris et al. [18] experimentally investigated the laminar flow convective heat transfer through a circular tube crossed with CuO–water and Al2O3–water. The obtained results show that the higher heat transfer enhancement is observed for Al2O3–water.Ruhani et al. [19]experimentally studied the new model for rheological behaviour of silica–ethylene glycol/water (30-70 vol.%) hybrid Newtonian nanofluid. The results indicate that as the volume fraction increases, the relative viscosity increases due to the greater dispersion of the nanoparticles in water. They found that when the relationship between shear stress and shear rate is linear, then the desired fluid is Newtonian. Abbasi et al. [20] investigated the blood flow in the presence of hybrid nanoparticles through a tapered complex wavy curved channel. The results show that the velocity of the blood is abated by the nanoparticle concentration and assisted in the non-uniform channel. Also, they found that the nanoparticle volume fraction and the dimensionless curvature of the channel reduce the temperature profile.

Recently, the control of nanofluid flow and forced convection heat transfer in channels is realised by the application of magnetic field. In this context, Mehrez and El Cafsi [21] studied the MHD forced convection of Al2O3–Cu/water hybrid nanofluid flow over a backward-facing step using the finite volume method. The obtained results show that the reattachment length is reduced when increasing nanoparticle volume fraction and by decreasing Reynolds number. The average Nusselt number increases by increasing volume fraction of nanoparticles and varies with the Hartmann number. Hussain and Ahmed [22] studied the MHD forced convection of Fe3O4-water in horizontal channel over a backward facing step including a rotating cylinder. The results show that the application of the electromagnetic force leads to diminution of the velocity of ferrofluid and improve the drag coefficient. Khan et al. [23] numerically investigated the impacts of Hartman number and variable thermal conductivity flow on velocity and temperature profile of Powell–Eyring fluid. The results show that the velocity profile enhances for larger magnetic parameter. Also, they found that the temperature profile decreases for increasing the Prandtl number (Pr), and enhances for increasing the value of thermal conductivity. Chu et al. [24] studied the impact of activation energy on bio-convection magnetohydrodynamic flow of third-grade fluid over a stretched subsurface. They found that the velocity field is declined when rising magnetic parameter. The thermal field and associated layer thickness is more subject to larger Brownian motion and thermophoresis parameters.

In another sense, researchers are very interested in the geometric form of the canal walls. In this context Pengand Peterson [25] experimentally studied the single-phase forced convective heat transfer and fluid flow in a microchannel with a small rectangular hot block. The obtained results show that the geometric configurations of the microchannel plate and individual microchannels have a critical effect on the single-phase convective heat transfer. The laminar and the turbulent convective heat transfer are quite different. Toghraie et al. [26] performed a 3D numerical study of convective heat transfer through a microconcentric annulus governing non-uniform heat flux boundary conditions employing water–Al2O3nanofluid. They showed that the model (when the exposing surface area is divided axially) leads to higher Nusselt numbers compared to the model when the exposing surface area is divided radially. Also, they found that the average Nusselt number is increased up to 142% and 83% when the exposing surface area is divided radially to eight parts with a Reynolds number

equal to 10 and when the model when the exposing surface area is divided axially to eight parts with a Reynolds number equal to 1,000, respectively. Moraveji and Toghraie [27] studied the impacts of a number of inlets, tube length and diameter of the cold outlet on temperature and on flow rates passing in the vortex tube. Their results showed that the increase in the diameter and the length of the vortex tube have positive impacts on the passing flow rate from a cold outlet. Also, they conclude that the temperatures at both outlets decreased as the number of inlets increased, while an increase is observed as the radius of the cold outlet is increased. Togun [28] numerically investigated simulation by using the finite volume method, the CuO–nanofluid and heat transfers in a backward-facing step with and without obstacles. The obtained results show that the maximum augmentation in heat transfer was about 22% for the backward-facing step with an obstacle of 4.5 mm and using CuO nanoparticles at a Reynolds number of 225 compared to the backward-facing step without an obstacle. It is also observed that the increase in the size of the recirculation region with an increase in the height obstacle on the channel wall has a remarkable effect on thermal performance. The results also found that the pressure drop increases by an increasing Reynolds number, obstacle height and volume fractions of CuO nanoparticles. Alamyane and Mohamad [29] investigated the forced convection heat transfer in a two-dimensional channel with extended surfaces, the computed results show that the spacing between extended surfaces and their height directly affects the heat transfer process, and the Nusselt number is decreased as the spacing is increased. In addition, as the Reynolds number increases the heat transfer rate also increases. Anas and Mussa [30] studied the forced convection in a channel with a wing shaped block using the finite volume method. The obtained results revealed that the heat transfer depends on the form of the block. Two directions of the flow are studied, and the maximum value of heat transfer is detected at the case when the flow comes from the left side. Yang et al. [31] investigated forced convection in a horizontal parallel plate channel with a transverse fin located at the lower wall using the control volume method. The obtained results show that the temperature profiles exhibit a great dependence on the value of ratio of fin length to fin height. Maia et al. [32] studied the forced convective heat transfer in laminar flow of non-Newtonian fluids in ducts with an elliptical section using the generalised integral transform technique (GITT). The obtained results exhibit a strong dependence of the heat transfer parameters with the aspect ratio. Khodabandeh et al. [33] analysed the heat transfer of water nanofluid/grapheme nanoplatelet–sodium in a microchannel in the presence of sinusoidal cavities with rectangular ribs. Their results showed that this configuration of the microchannel can have a substantial increase in the Nusselt number and heat transfer. The average Nusselt number increases about 20% when the nanoparticle mass fraction is equal to 0.1% compared with the base fluid. Fanambinantsoa et al. [34] investigated the forced convection in a rectangular channel with a sinusoidal protuberance. They concluded that a change in the magnitude of the protrusion significantly affects the heat transfer. Besides, the heat transfer is more intense in the area where the vortex zones are created. Buyruk and Karabulut [35] analysed numerically (FLUENT) the heat transfer in a rectangular channel filled with air for different types of fins. The results show that the pressure drop increases when using a channel with zigzag on the lower plate compared to the flat channel. Dixit and Patil [36] experimentally investigated the heat transfer between two plates with three forms

of fins such as simple fins, fins with inclined groove (V) and fins with multiple (V). The results show that the fin with inclined groove had the highest value of enhancement among all fin types. Most of the research studies cited before considered the importance of the geometric shape of the obstacle in heat transfer, and the obtained results show that the complexity of the shape of the obstacle implies a variation in the heat transfer rate.

Entropy generation is among the most important parameters in heat transfer problems [37–41], and it was found that the total entropy generation number depends on many parameters such as the volume fraction of nanoparticles, Reynolds number and Hartmann number.

In the present work, 2D numerical simulations of the MHD forced convective flow in a channel with a heat source and the partially heated walls are studied. The novelty of this work compared to the existing literature is the study involving nanoliquid forced convection with different boundary conditions (insulated–hot–insulated–hot–insulated) and the position of the hot block, which is placed inside the channel. This position is optimised based on the calculation of entropy generation. To the authors' best knowledge, this study is not undertaken in the open literature in the presence of uniform magnetic field. For this specific problem, Brownian motion is taken into account and compared with the cases without Brownian motion. Also, this study gathers many other studies dealing with the Reynolds effect, Hartman number effect, nanoparticle concentration effect, nanoparticle diameter effect and magnetic field inclination angle effect.

2. PROBLEM STATEMENT

The physical problem of the current study consists of a two-dimensional channel of length L and height H (L/H=6) crossed by Cu–water nanoliquid and containing a heat source Fig. 1.

The nanoliquid flow is driven along the channel by a constant velocity Uin and a cold temperature Tin at the inlet. Parts of the channel walls, located near the entrance, the middle and the outlet of the channel are insulated (L1=L2/2 and L2=L3=b). At the remaining parts, a uniform temperature of nanoliquid flow is equal to 1 (Tw=1). A uniform magnetic field is applied. Its orientation forms an angle γ with the horizontal plate. The nanoliquid is simulated using the single-phase model, Newtonian, laminar and incompressible. The thermo-physical properties of water and Cu nanoparticles are displayed in Tab.1.

Tab. 1. Physical properties of water and Cu nanoparticles [7] at 20°C

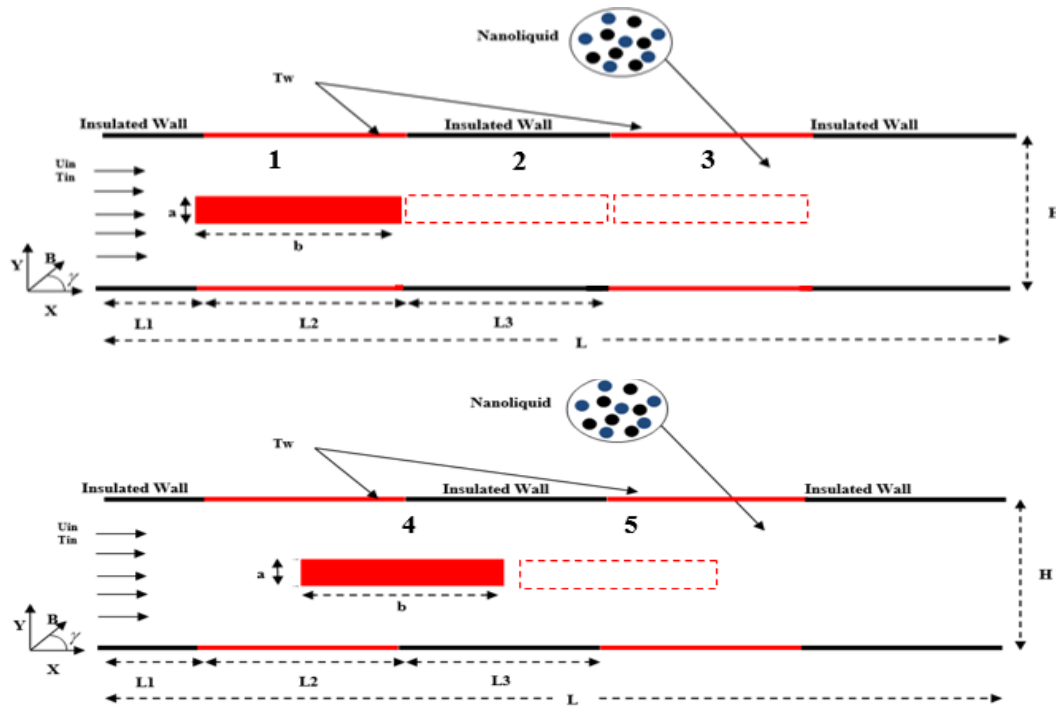| Physical property	Water	Cu
$Cp(J.kg^{-1}.K^{-1})$	4181.8	383.1
$\rho(kg.m^{-3})$	1,000.52	8,954
$k(W.m^{-1}.K^{-1})$	0.597	386
$\beta(K^{-1})$	21×10^{-5}	51×10^{-6}
$\sigma(\Omega.m)^{-1}$	0.05	2.7×10^{-8}
$\mu \times 10^4 (kg/m.s)$	8.55	-

Fig. 1. Physical configuration

3. MATHEMATICAL FORMULATION AND BOUNDARY CONDITIONS

3.1. Mathematical formulation

The governing Eqs (1–4) are made dimensionless using the following variables:

$$X = \frac{x}{H}, Y = \frac{y}{H}, U = \frac{u}{u_{in}}, V = \frac{v}{u_{in}}, Pr = \frac{v_{nl}}{\alpha_{nl}},$$

$$\theta = \frac{T - T_{in}}{T_w - T_{in}}, Re = \frac{u_{in} D_h}{v_{nl}}, P = \frac{p}{u_{in}^2}, Ha = HB_0 \sqrt{\frac{\sigma_{nl}}{\mu_{nl}}}$$

Accordingly, the governing equations are given as follows:

$$\frac{\partial U}{\partial X} + \frac{\partial V}{\partial Y} = 0 \tag{1}$$

$$U \frac{\partial U}{\partial X} + V \frac{\partial V}{\partial Y} = -\frac{\partial P}{\partial X} + \frac{1}{Re} \left(\frac{\partial^2 U}{\partial X^2} + \frac{\partial^2 U}{\partial Y^2} \right) +$$
$$\frac{Ha^2}{Re} \left(V \sin(\gamma) \cos(\gamma) - U \sin^2(\gamma) \right) \tag{2}$$

$$U \frac{\partial V}{\partial X} + V \frac{\partial V}{\partial Y} = -\frac{\partial P}{\partial Y} + \frac{1}{Re} \left(\frac{\partial^2 V}{\partial X^2} + \frac{\partial^2 V}{\partial Y^2} \right) +$$
$$\frac{Ha^2}{Re} \left(U \sin(\gamma) \cos(\gamma) - V \cos^2(\gamma) \right) \tag{3}$$

$$U \frac{\partial \theta}{\partial X} + V \frac{\partial \theta}{\partial Y} = \frac{1}{Pr.Re} \left(\frac{\partial^2 \theta}{\partial X^2} + \frac{\partial^2 \theta}{\partial Y^2} \right) \tag{4}$$

4. BOUNDARY CONDITIONS

At the inlet of channel,

$$U = 1; V = 0; \theta = 0 \tag{5}$$

At the outlet of channel,

$$\frac{\partial U}{\partial x} = \frac{\partial V}{\partial x} = 0 \tag{6}$$

$$\frac{\partial \theta}{\partial x} = 0 \tag{7}$$

At the hot block,

$$U = 0; V = 0; \theta = 1 \tag{8}$$

5. NUMERICAL PROCEDURE

5.1. Solution method

The LBM has been successfully used in various classic and emerging scientific and engineering fields [29, 41, 48]. LBM has several advantages over other conventional CFD methods, especially in dealing with complex boundaries, incorporating microscopic interactions and parallelisation of the algorithm. A different interpretation of the lattice Boltzmann equation (LBE) is that of a discrete-velocity Boltzmann equation. The numerical methods for the solution of partial differential equations give rise to a discrete map, which can be interpreted as the propagation and collision of fictitious particles. To simulate flow and heat transfer in a two-dimensional channel, the LBM is used with the D2Q9 model Fig. 2 (a) for the dynamic field and with the D2Q4 for the thermal field Fig. 2 (b), and the selected grid size is uniform ($\Delta x = \Delta y = 1$).

The LBE with an external term force is solved using the BGK approximation. Consequently, the obtained LBE with a single relation time is written as follows:

$$f_k(x + c_k \Delta t, t + \Delta t) =$$
$$f_k(x, t) + \frac{\Delta t}{\tau} \left[f_k^{eq}(x, t) - f_k(x, t) \right] + \Delta t F_k \tag{9}$$

where $\Delta t, \tau, c_k, F_k$ and f_k^{eq} denote, respectively, the lattice time step, relaxation time, discrete lattice velocity in direction (i), external force in the direction of lattice velocity and the equilibrium distribution function.
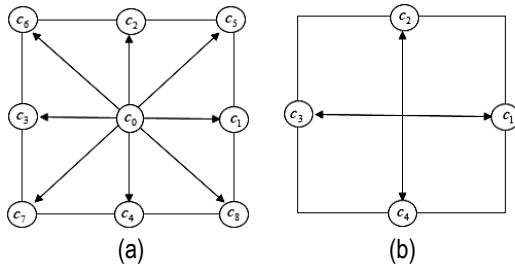

Fig. 2. D2Q9- D2Q4 models: for the velocity field (a) and for temperature field (b)

5.2. LBE for dynamic and thermal fields

For the dynamic field,

$$f_k(x + c_k\Delta t, t + \Delta t) = f_k(x,t) + \frac{\Delta t}{\tau_v}\left[f_k^{eq}(x,t) - f_k(x,t)\right] + \Delta t c_k F_k \tag{10}$$

For the temperature field,

$$g_k(x + c_k\Delta t, t + \Delta t) = g_k(x,t) + \frac{\Delta t}{\tau_g}\left[g_k^{eq}(x,t) - g_k(x,t)\right] \tag{11}$$

where τ_v and τ_g are the relaxation times for the flow and temperature fields, and f_k^{eq} and g_k^{eq} are the equilibrium distribution functions given for the D2Q9-D2Q4 models, respectively, which are given as follows:

$$f_k^{eq} = \rho\omega_k\left[1 + 3\frac{c_k.u_i}{c^2} + \frac{9(c_k.u_i)^2}{2c^4} - \frac{3u_i^2}{2c^2}\right] \tag{12}$$

$$g_k^{eq} = 0.25\theta[1 + 2c_k.u_i] \tag{13}$$

For the D2Q9, the weighting factors and the discrete particle velocity vectors are defined as follows:

$$\begin{pmatrix} \omega_k \\ c_{k,x} \\ c_{k,y} \end{pmatrix} = \begin{pmatrix} \frac{4}{9}, \frac{1}{9}, \frac{1}{9}, \frac{1}{9}, \frac{1}{9}, \frac{1}{36}, \frac{1}{36}, \frac{1}{36}, \frac{1}{36} \\ 0, 1, 0, -1, 0, 1, -1, -1, 1 \\ 0, 0, 1, 0, -1, 1, 1, -1, -1 \end{pmatrix}$$

The macroscopic quantities are calculated by the following equations:

$$\rho(x,y) = \sum_{k=0-8} f_k \tag{14}$$

$$\rho u(x,t) = \sum_{k=0-8} f_k c_k + \Delta t F \tag{15}$$

$$\theta = \sum_{k=0-4} g_k \tag{16}$$

5.3. LB boundary condition treatment

One of the important and crucial issues in LBM simulation of flow and temperature is accurate modelling of the boundary conditions.

5.3.1. Hydrodynamic boundary conditions

At the inlet, the unknown distribution functions are calculated using the boundary condition proposed by Zou and He[42] as follows:

$$\rho_{in} = \frac{f_0 + f_1 + f_2 + f_4 + 2(f_3 + f_6 + f_7)}{1 - u_{in}} \tag{17}$$

$$f_1 = f_3 + \frac{2}{3}\rho u_{in} \tag{18}$$

$$f_5 = f_7 + \frac{1}{2}(f_4 - f_2) + \frac{1}{6}\rho u_{inlet} \tag{19}$$

$$f_8 = f_6 + \frac{1}{2}(f_4 - f_2) + \frac{1}{6}\rho u_{inlet} \tag{20}$$

At the outlet, a second-order extrapolation scheme is used by Mohamad [43]:

$$f_3(n,j) = 2 \times f_3(n-1,j) - f_3(n-2,j) \tag{21}$$

$$f_6(n,j) = 2 \times f_6(n-1,j) - f_6(n-2,j) \tag{22}$$

$$f_7(n,j) = 2 \times f_7(n-1,j) - f_7(n-2,j) \tag{23}$$

The bounce-back boundary condition is applied on all solid boundaries. For instance, for the top boundary, the following conditions are imposed:

$$f_4(i,m) = f_2(i,m) \tag{24}$$

$$f_7(i,m) = f_5(i,m) \tag{25}$$

$$f_8(i,m) = f_6(i,m) \tag{26}$$

5.3.2. Thermal boundary conditions

At the inlet,

$$g_1 = \theta\big(\omega(1) + \omega(3)\big) - g_3 \tag{27}$$

$$g_5 = \theta\big(\omega(5) + \omega(7)\big) - g_7 \tag{28}$$

$$g_8 = \theta\big(\omega(8) + \omega(6)\big) - g_6 \tag{29}$$

At the outlet,

$$g_3(n,j) = 2 \times g_3(n-1,j) - g_3(n-2,j) \tag{30}$$

$$g_6(n,j) = 2 \times g_6(n-1,j) - g_6(n-2,j) \tag{31}$$

$$g_7(n,j) = 2 \times g_7(n-1,j) - g_7(n-2,j) \tag{32}$$

At the insulated part of the walls, the bounce-back boundary condition (adiabatic) is used on the north and the south boundaries. For instance, for the top boundary, the following conditions are imposed:

$$g_4(i,m) = g_4(i,m-1) \tag{33}$$

$$g_7(i,m) = g_7(i,m-1) \tag{34}$$

$$g_8(i,m) = g_8(i,m-1) \tag{35}$$

At the heated part of the walls, the temperature is known, θ=1, for instance, for the top wall, and the following conditions are imposed:

$$g_4 = \theta\big(\omega(4) + \omega(2)\big) - g_2(i,m) \tag{36}$$

$$g_7 = \theta\big(\omega(7) + \omega(5)\big) - g_5(i,m) \tag{37}$$

$$g_8 = \theta\big(\omega(8) + \omega(6)\big) - g_6(i,m) \tag{38}$$

5.4. Nanoliquid property calculation

The terms $(\rho Cp)_{nl}, \rho_{nl}, \alpha_{nl}$, the heat capacitance, nanoliquid density and the thermal diffusivity are approximated as follows [39]:

$$(\rho Cp)_{nl} = (1 - \phi)(\rho Cp)_l + \phi(\rho Cp)_p \tag{39}$$

$$\rho_{nl} = (1 - \phi)\rho_l + \phi\rho_p \tag{40}$$

$$\alpha_{nl} = k_{nl}/(\rho Cp)_{nl} \tag{41}$$

Thermal conductivity is given by Koo and Kleinstreuer [45]:

$$k_{nl} = k_{static} + k_{Browinan} \tag{42}$$

where the static thermal conductivity is based on the Maxwell classical equation:

$$k_{static} = k_l \frac{k_p + 2k_l - 2\phi(k_l - k_p)}{k_p + 2k_l + \phi(k_l - k_p)} \tag{43}$$

The thermal conductivity is due to the enhanced thermal conductivity by micro-scale convective heat transfer of a particle's Brownian motion:

$$k_{Brownian} = 5 \times 10^4 \beta\phi\rho_l Cp_l \sqrt{\frac{k_b T}{\rho_p d_p}} f(T, \phi) \tag{44}$$

where β and f are two functions that combine the interaction between nanoparticles:

$$\beta = 0.0137(100\phi)^{-0.8229} \, for \, \phi < 1\% \tag{45}$$

$$\beta = 0.0011(100\phi)^{-0.7272} \, for \, \phi > 1\% \tag{46}$$

$$f(T, \phi) = (-6.04\phi + 0.4705)T + \tag{47}$$

$$(1.7223\phi - 134.63) \, for \, 1\% \le f \le 4\%$$

This equation is valid for temperatures in the range of $300K \le T \le 325K$.

The effective viscosity of the nanoliquid is given by Koo and Kleinstreuer as [44, 45]:

$$\mu_{eff} = \mu_{static} + \mu_{Brawnian} \tag{48}$$

where μ_{static} is the static viscosity of the nanoliquid and $\mu_{Brownian}$ is the effective viscosity due to Brownian motion:

$$\mu_{static} = \frac{\mu_l}{(1 - \phi)^{2.5}} \tag{49}$$

$$\mu_{Brownian} = 5 \times 10^4 \beta\phi\rho_l \sqrt{\frac{k_b T}{\rho_p d_p}} f(T, \phi) \tag{50}$$

The electrical conductivity of the nanoliquid is giving by Maxwell's model:

$$\sigma_{nl} = \sigma_l \left[1 + \frac{3(\sigma_s/\sigma_l - 1)\phi}{(\sigma_s/\sigma_s + 2) - (\sigma_s/\sigma_l - 1)\phi}\right] \tag{51}$$

5.5. Physical quantities of interest

5.5.1. Nusselt number

The convective heat transfer is described using the local and average Nusselt number along the hot wall, and the local Nusselt number is expressed as follows:

$$Nu = -\frac{k_{nl}}{k_l}\left(\frac{\partial \theta}{\partial Y}\right)\Big|_{Y=0} \tag{52}$$

The average Nusselt number is expressed as follows:

$$Nu_{avg} = \frac{1}{L}\int_0^L Nu \, dX \tag{53}$$

where L is the channel length.

5.5.2. Entropy generation:

The local dimensionless entropy generation is the result of the sum of the irreversible heat transfer, fluid friction and magnetic field [46]:

$$S_{gen} = S_{gen,h} + S_{gen,v} + S_{gen,M} \tag{54}$$

The first term relative to the heat transfer irreversibility is as follows:

$$S_{gen,h} = \frac{k_{nl}}{k_l}\left[\left(\frac{\partial \theta}{\partial X}\right)^2 + \left(\frac{\partial \theta}{\partial Y}\right)^2\right] \tag{55}$$

The second term corresponding to the fluid friction irreversibility is as follows:

$$S_{gen,v} = \chi \frac{\mu_{nl}}{\mu_l}\left\{2\left[\left(\frac{\partial U}{\partial X}\right)^2 + \left(\frac{\partial V}{\partial Y}\right)^2\right] + \left[\left(\frac{\partial U}{\partial Y}\right) + \left(\frac{\partial V}{\partial X}\right)\right]^2\right\} \tag{56}$$

The last term associated with the magnetic field irreversibility is as follows:

$$S_{gen,M} = \chi \times Ha^2 \times \left[(1 - \phi) + \phi\frac{\rho_s}{\rho_l}\right]$$
$$\times [U\sin(\gamma) - V\cos(\gamma)]^2 \tag{57}$$

where χ represents the irreversibility factor and is given by [45]:

$$\chi = \frac{\mu_l T_{in} U_{in}^2}{k_l(T_w - T_{in})^2} \tag{58}$$

The Bejan number (Be), which is important while discussing the entropy generation, is defined as the ratio of entropy generations due to heat transfer and total entropy generation:

$$Be_{Local} = \frac{S_{gen,h}}{S_{gen}} \tag{59}$$

The total entropy generation, S_{gen}, and the Bejan number, Be, are calculated by the integration over the whole domain Ω as follows:

$$S_{gen} = \iint_\Omega S_{gen} dXdY \, and \, Be = \iint_\Omega Be_{local} dXdY \tag{60}$$

6. GRID INDEPENDENCE TEST AND CODE VALIDATION

The grid sensitivity is tested to let our code giving accurate independent solution. Tab. 2 shows the effect of grid size on the Nuavg through the two-dimensional channel. The grid node 60x360 is the appropriate and is selected for the next computations.

The case of two-dimensional heated channel crossed with cold air (Pr=0.71) was taken as a benchmark test in order to ensure that the obtained results are reliable. The channel was heated from its top and bottom walls.

Tab. 2. Dependence of Nu$_{avg}$ on mesh resolution
for Re = 150 and ϕ= 0.02

Mesh	30 x 180	60 x 360	90 x 540	120 x 720
Nu_{avg}	12.32	11.65	11.73	11.97

First, the velocity profiles at different sections of the channel are compared with those obtained by [37-47-48](Fig. 3) (a). Second, the velocity profile are compared to the analytical solution for the fully developed flow between two parallel plates Fig. 3 (b). Results show a good agreement for the two cases. We conclude that the results of Fortran code calculations are acceptable.
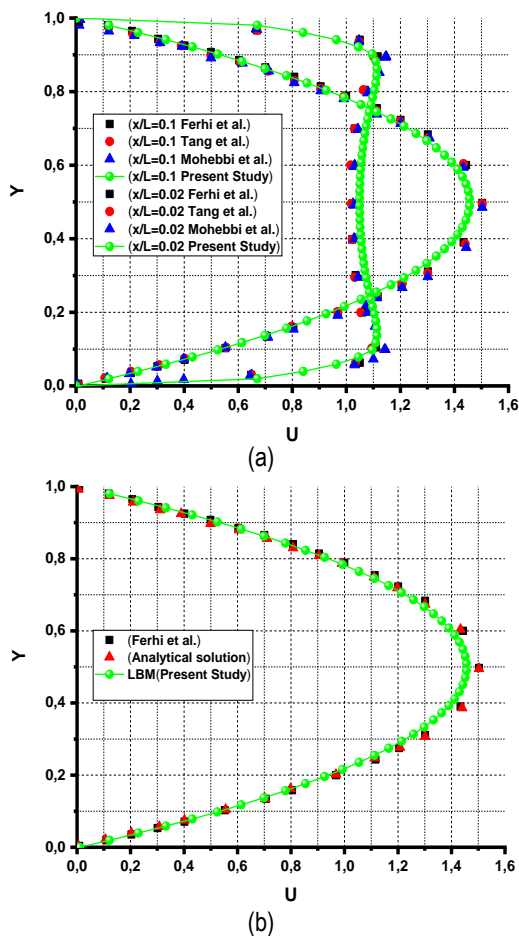

(a)

(b)

Fig. 3. Comparison of the velocity profiles at different channel sections with literature findings (a) and analytical solution (b)

7. RESULTS AND DISCUSIONS

In the following sections, a numerical investigation has been carried out to appraise the effects of emerging parameters on the MHD hydrodynamic and thermal characteristics and entropy generation inside a channel crossed by Cu–water nanoliquid with a constant velocity and driven by a cold temperature at the inlet containing a heat source. Particular efforts have been focused on the effects of key parameters such as Reynolds number (Re =50–200), nanoparticle volume fraction ($\phi = 1\% - 4\%$), nanoparticle diameter (dp=5–45nm), Hartmann number (Ha =0–90) and the magnetic field inclination angle ($\gamma = 0 - \pi$), on the convective nanoliquid flow, heat transfer and the second law analysis inside the studied configuration. The Brownian motion is taken into consideration via the theoretical models of Koo and Kleinstreur (43) for nanoliquid thermal conductivity and dynamic viscosity. In this study, the case in which the heat source is placed in the middle of the channel (case 2) is adopted, due to the maximum value of the average Nusselt number detected in this position of the block.

7.1. Heat source position effects

Fig. 4 presents the variation of the heat transfer as a function of the heat source position. It is seen that the heat transfer, which is described by the average Nusselt number, is minimum when the heat source is placed near the insulated wall. In this position, the heat exchange is produced only between the heat source and the nanoliquid. The heat exchange is remarkable when the heated block is placed near the active walls. The heat transfer is transferred by convection between the heat source and the walls of the channel by means of the nanoliquid. Besides, the nanoliquid is rapidly heated by the heat source and the walls.
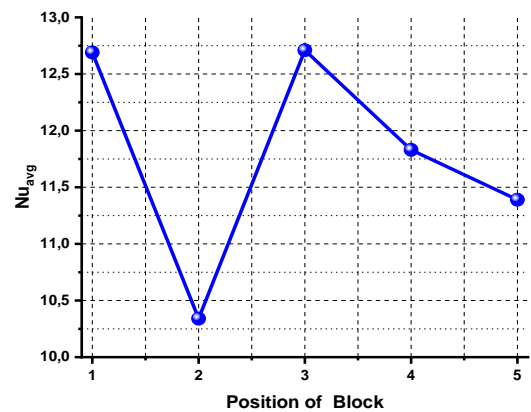

Fig. 4. Variation of average Nusselt number for different positions of the heated obstacle

7.2. Nanoparticle volume fraction effects

Fig. 5 shows the effect of the copper nanoparticle volume fraction on the heat transfer (a), Sgen (b) and Be (c) for different Re numbers at Ha=50, dp=25nm and $\gamma = 0$. It is seen clearly that the increase in ϕ leads to enhance the heat transfer in the bottom wall. Besides, the addition of nanoparticles to the base fluid caus-

sciendo

Rached Miri, Mohamed A. Abbassi, Mokhtar Ferhi, Ridha Djebali
Second Law Analysis of MHD Forced Convective Nanoliquid Flow Through a Two-Dimensional Channel

DOI 10.2478/ama-2022-0050

es the augmentation of the thermal conductivity in the channel consequently the heat transfer increases Fig. 5 (a).

The impact of the nanoparticle volume fraction on the entropy generation for different Re numbers is depicted in Fig. 5 (b). The enhancement of heat transfer increases the total entropy generation in the channel. Besides, as ϕ increases, the heat transfer and the viscosity of the mixture in the medium increase, this led to improve the heat transfer and the fluid friction irreversibility. The evolution of the Be number versus the nanoparticle volume fraction is illustrated in Fig. 5 (c). The Be number increases as ϕ increases. This result indicated that the convective mode is dominant. It can be concluded that the profiles of Nuavg, Sgen and Be increase, and these performances are due to enhancing the thermal conductivity of nanoliquid.
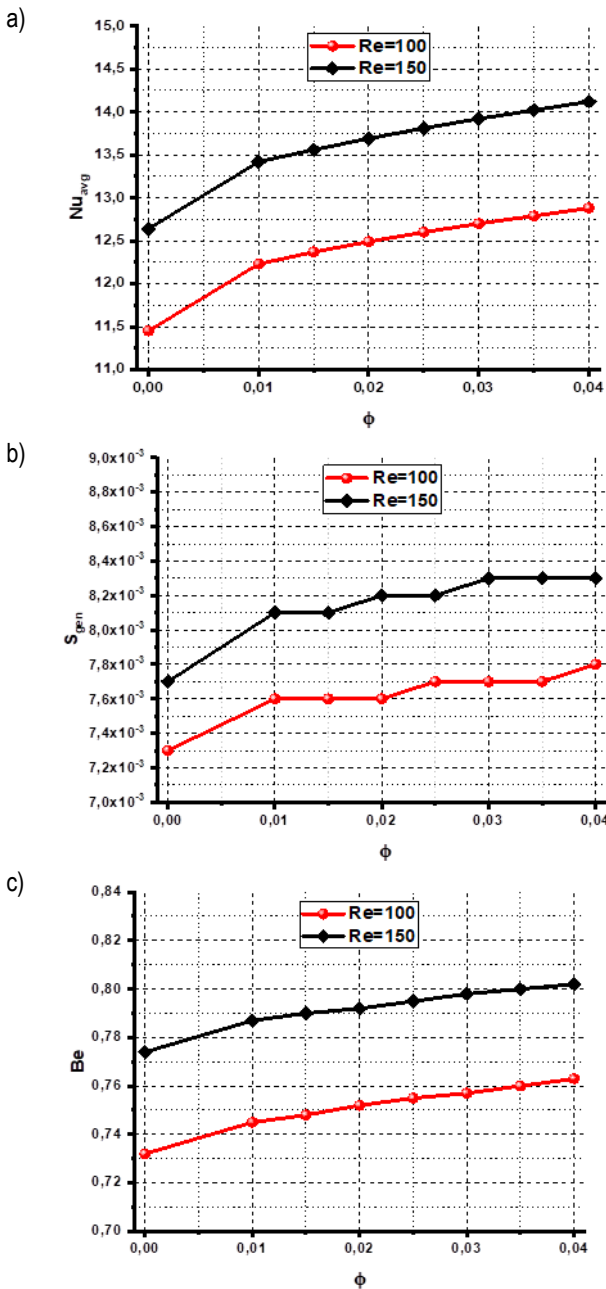
7.3. Nanoparticle size effects

Fig. 6 describes the influence of nanoparticle diameter on Nuavg (a), Sgen (b) and Be (c) for different nanoparticle volume fraction at Re =150, Ha=50 and $\gamma = 0$. It is clear that the augmentation of the nanoparticle diameter leads to a decrease in the heat transfer, the entropy generation and the Bejan number in the entire of the channel. We noticed that the curve can be divided into two zones: in the first zone (5nm<dp<35nm), the calculated parameters (Nuavg, Sgen and Be) are decreasing and degrade rapidly, but in the second zone (dp>35nm), the curve tends towards stabilisation. In case of nanoliquid, decreasing dp leads to a higher heat transfer rate as a result of a higher heat transfer surface area (contact area between particles and liquid), aggregation of nanoparticles and more intensified Brownian motion, causing higher thermal conductivity of the nanoliquid. At a fixed volume fraction and decreasing dp, the particle number increases, which augments the total surface and therefore contributes to the rise of nanoliquid thermal conductivity.
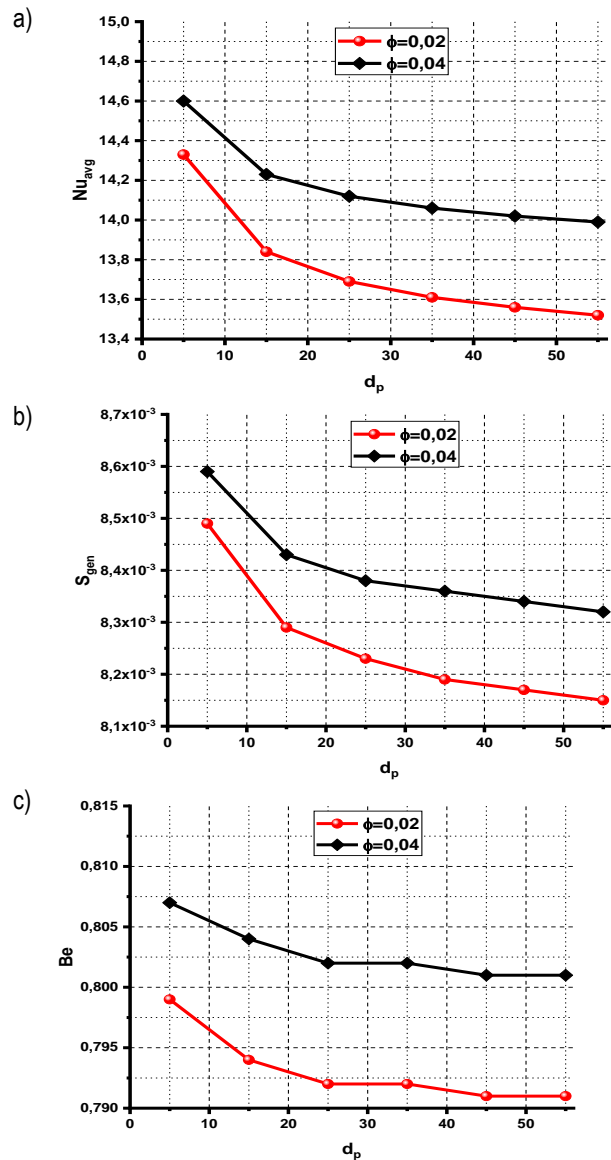

Fig. 5. Variations of the Nuavg; a) Sgen; b) and Be; c) as a function of nanoparticles volume fraction for different Re numbers for Ha = 50, dp = 25 nm and $\gamma = 0$

Fig. 6. Variations of the Nuavg; a) Sgen; b) and Be; c) as a function of nanoparticle diameter for Re = 150, Ha = 50 and $\gamma = 0$

7.4. Reynolds number effects

Fig. 7 illustrates the effects of Re numbers on the streamlines (left) and isotherms (right) for $\phi = 2\%$, dp=25 nm and Ha=50. As Re increases, a recirculation zone appears behind the heat source Fig. 7 (left). The size and shape of this zone depend on the shape of the obstacle and the Reynolds number.

Fig. 7 (left) presents the streamlines, and the increase in the Reynolds number has a direct influence on the streamlines, and the lines are more compact when the Reynolds numbers increase, and this is due to the enhancement of the inertial force. This can be clearly seen in the velocity profile illustrated in Fig. 8.

Fig. 7 (right) presents the distribution of the isotherms in the nanoliquid. The figure indicates that the evolutionary temperature contours break down when the Re number of nanoliquid is increased, and this due to reduction of the boundary layer. The convection mechanism becomes stronger and isotherms are distorted, so temperature gradient near the hot surface augments.
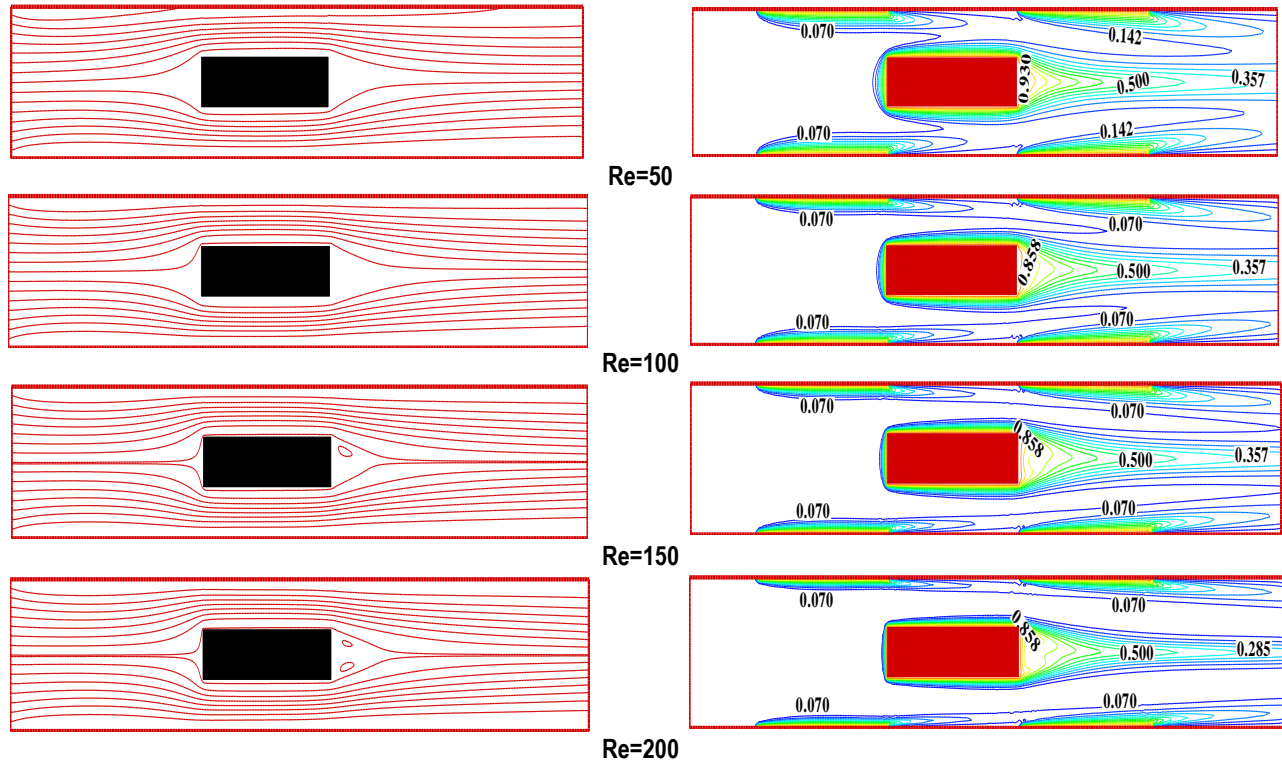

Re=50

Re=100

Re=150

Re=200

Fig. 7. Streamlines (left) and isotherms (right) for different Reynolds numbers at $\phi = 0.02$, Ha = 50 and γ = 0

Fig. 8 shows the variation of Nuavg (a), Sgen (b) and Be (c) as a function of Reynolds numbers. The augmentation of Re numbers causes to increase the average Nusselt number, and consequently, the curve of total entropy generation and the Bejan number of the nanoliquid increase.

In Fig. 8 (a), the Nuavg enhances by 20% when Re numbers increase from 50 to 190. The heat transfer of nanoliquid increases linearly as a function of Re. As a result, the heat transfer due to the convective mode is dominated.

Fig. 8 (b) depicts the evolution of the total entropy generation as a function of Reynolds numbers. It is shown from the figure that at a low Reynolds number, the total entropy generation decreases, and the minimum value of the total entropy generation is detected for Re=80 equal to $S_{gen} = 7.55 \times 10^{-3}$. This decrease of the curve is caused by the passage of the flow between two cold walls, and also because of the decrease of the first term of equation (54). For $Re > 80$, the heat transfer due to the convective mode dominates. There is an increase in the velocity of the nanoliquid and, by consequence; the second term of Eq. (54) dominates the other term of the equation, which indicates a linear increase in the curve of the total entropy generation as a function of the Reynolds number.

The impact of Reynolds numbers on the Bejan number is illus-

trated in Fig. 8 (c). It is found that the curve of the Bejan number as a function of the Reynolds number tends towards stability. This result is due to augmentation of the term relative to heat transfer irreversibility.

Comparing nanoliquid with $\phi = 0.04$ to the nanoliquid with $\phi = 0.02$, it shows that when adding low-volume fractions of nanoparticles and/or increasing Reynolds number causes higher frictional entropy generation. The addition of low-volume fractions of nanoparticles intensifies the hydrodynamic inter-particle interactions, causing a higher viscosity of the nanoliquid. This result is due to higher thermal conductivity of nanoparticles. Based on Eq. (55), the thermal entropy generation is related to temperature gradients. By increasing the nanoparticle volume fraction, the nanoliquid viscosity increases, which makes conventionalliquid molecules slower and creates a smoother temperature profile by stabilising the flow field.

Fig. 9 describes the variation of the velocity profiles along the vertical centreline (a) and the horizontal velocity (b) for different Reynolds numbers (Re=50,100,150), Ha=50 and γ=0. The figure reveals that the rise in Re reduces the velocity in the regions between the walls and the heat source. Fig. 9 (a). The curve is divided into three sections: one is linear, and the other are two parabolic and symmetric sections. The increase in the Reynolds number gives results in a decrease in the amplitude of the vertical

Rached Miri, Mohamed A. Abbassi, Mokhtar Ferhi, Ridha Djebali
Second Law Analysis of MHD Forced Convective Nanoliquid Flow Through a Two-Dimensional Channel

DOI 10.2478/ama-2022-0050

velocity profile (direction Y), and on the other hand, the amplitude of the horizontal velocity profile (direction X) increases.
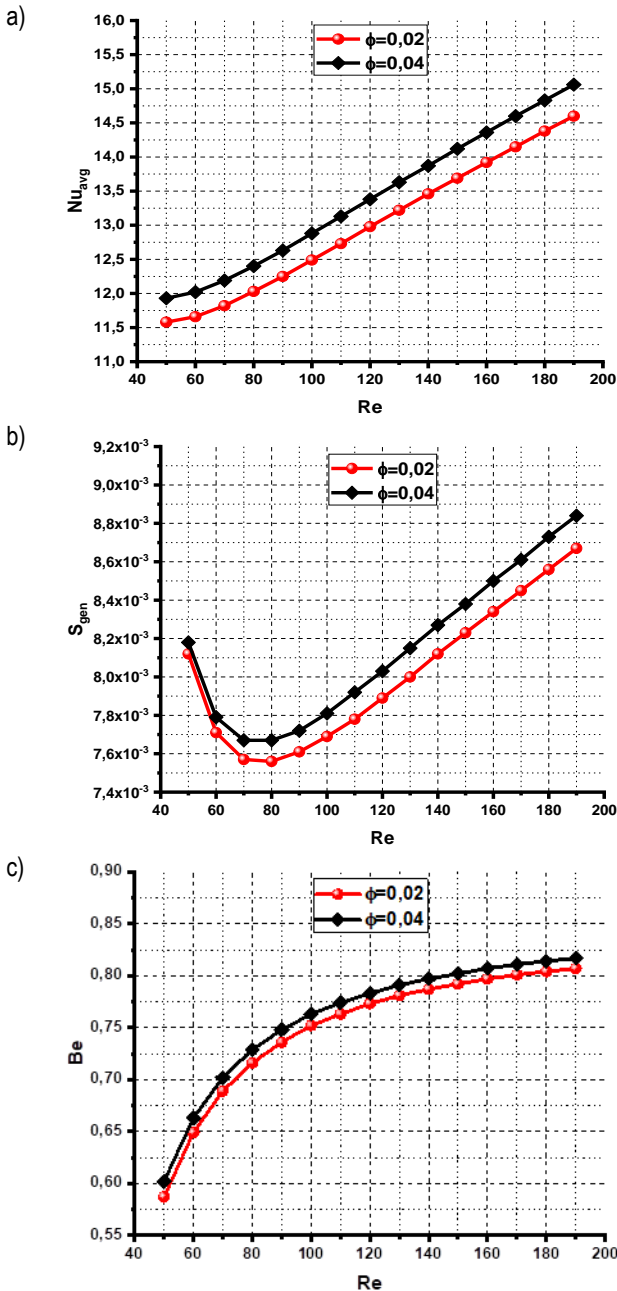

a)

b)

c)

Fig. 8. Variations of the Nu_{avg}; a) S_{gen}; b) and Be; c) as a function of Re numbers for Ha = 50 and γ = 0

The profile of the dimensionless horizontal velocity of the nanoliquid along the channel centreline for different Reynolds numbers (Re=50,100,150), Ha=50 and $\gamma = 0$ is depicted in Fig. 9 (b). Four zones are in this curve: in the first zone ($0 \leq X \leq 0.33$) as Re numbers increase, the velocity component and the amplitude of the velocity component for the nanoliquid increase, and the minimum value of velocity increases about 38.7% when the number of Reynolds increases from 50 to 150. For this zone, the velocity profile is slightly increased; this is due to the passage of the nanoliquid between two cold walls when the slip velocity increment of the nanoliquid velocity on boundaries. To conclude, the impact of inertial forces dominates in this zone.

In the second zone ($0.33 < X < 0.55$), the velocity profile is equal to zero because of the presence of the obstacle in the middle of the channel.

The third zone ($0.55 \leq X \leq 0.61$) when the recirculation zone is obtained, as Re number decreases, the amplitude of the velocity profile for nanoliquid increases. In this zone, the sign of the velocity component changes from positive to negative, and the minimum value of velocity increases by 59.3% when the number of Reynolds increases from 50 to 150. The inertial forces decrease, and the impact of viscous forces is presented.

The last zone ($0.61 < X \leq 1$) and for the height Reynolds number, the minimum value of velocity increases about 99.98% when the number of Reynolds increases from 50 to 150. This is due to the heat recirculation zone formed behind the block, and it is responsible for changing the sign of the velocity. In this zone, the heat transfer due to the conductive mode dominates.

We noticed that the velocity profile depends on the number of Reynolds, in both zones after and before the position of the obstacle. As the first zone, the velocity profile is slightly increased, which is due to the domination of conductive mode. On the other side and after the position of the recirculation zone, the velocity profile of the nanoliquid increases rapidly in the same distance, this is due to the passage of flow between the hot walls and the contact with the outside surface of the hot obstacle. So the boundary condition plays a very important role in increasing or decreasing the flow rate of nanoliquids; therefore, the viscous force directly depends on the limiting condition imposed on the walls of the channel.
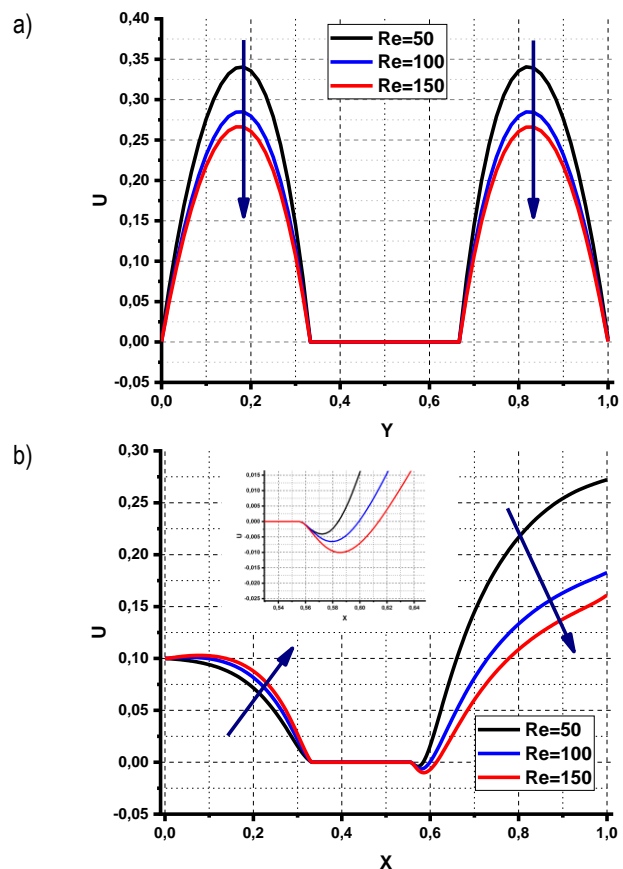

a)

b)

Fig. 9. U(0.5, Y); a) U(X, 0.5); b) and θ(X, 0.5) for different Reynolds numbers at Ha = 50 and γ = 0

7.5. Effect of Hartmann number

Fig. 10 presents the evolution of Nuavg (a), Sgen (b) and Be (c) as a function of Hartmann number for two Re numbers (100 and 150). It is seen that heat transfer is enhanced by increasing Ha for all values of Re number. Fig. 10 (a). For example, for a Reynolds number equal to 100, the inertia force deepens by the heightening of the magnetic field. This fact increases the convective heat transfer mode.

The impact of magnetic field intensity on the Sgen and Be number is depicted in Fig. 10 (b) and (c). It is clear that the total entropy generation increases as the Ha number increases. In this curve, we have detected an intersection, and this intersection can be interpreted by the presence of the recirculation zone, and it has been detected when Re is greater than 100, and this zone has an opposite effect to the Reynolds number.
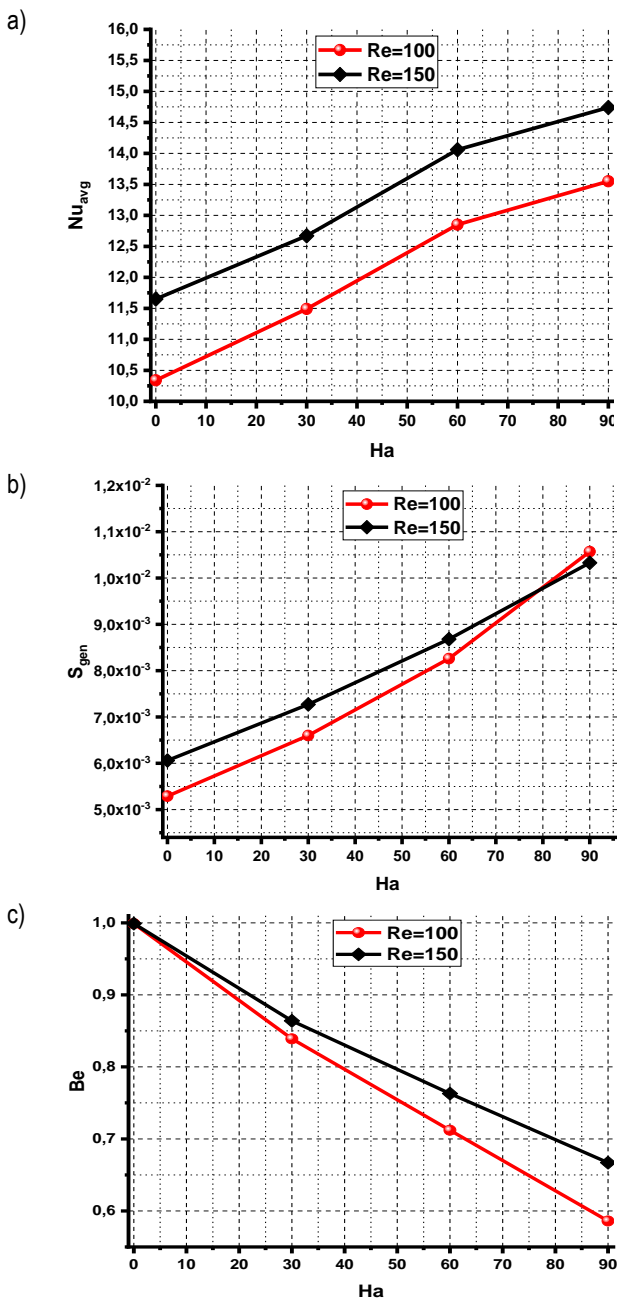
Fig. 10 (c) depicts the variation of the Be number in the function of Hartmann number, and it shows that the mode of heat transfer changes from conduction to convection. Besides, the Be is reduced by 41.4% for Re=100, while the Be is reduced by about 33.3% for Re= 150. This happens when the Ha increases from 0 to 90. This is due to augmentation of the term relative to the heat transfer irreversibility Eq. (55).
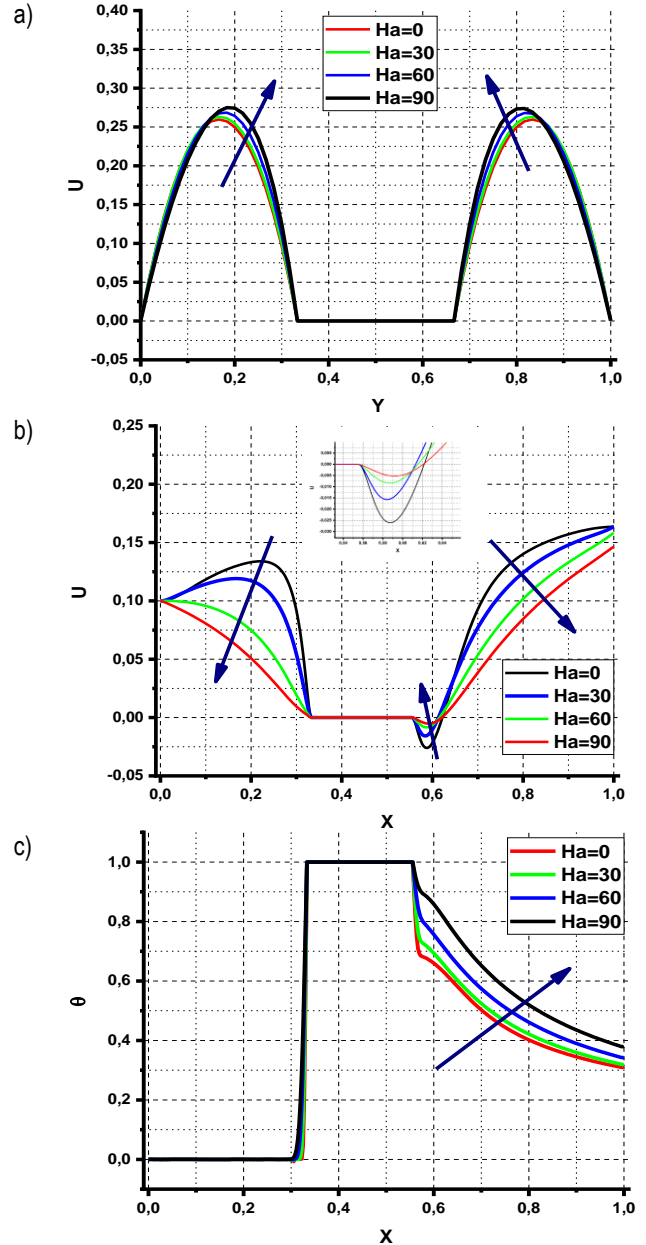

Fig. 11. U(0.5, Y); a) U(X, 0.5); b) and θ(X, 0.5); c) for different Ha numbers at Re = 150, $\phi = 0.02$, dp = 25 nm and $\gamma = 0$

Fig. 11 describes the variation of the velocity profiles along the vertical centreline (a), the horizontal velocity (b) and the temperature profile in the X direction for Ha=0,30,60,90 and Re=150. It shows that the flow is fully developed with two parabolic profiles. It is noted that the Ha number causes an improvement of the velocity in the zone between the heat source and the channel walls. Fig. 11 (a). When increasing the Hartmann number, a positive effect of electromagnetic force is shown, so the amplitude of vertical velocity increases.

Fig. 10. Variations of the average Nusselt number; a) S_gen ;b) and Be; c) as a function of Ha numbers for $\phi = 2\%$ and $\gamma = 0$

Fig. 11 (b) illustrates the dimensionless horizontal velocity profiles in the X direction for different values of Hartmann number (Ha=0, 30, 60 and 90), and it shows that the velocity profile is maximum when Ha=0. Four zones in this curve are shown, and the first zone is situated between $(0 \leq X \leq 0.33)$. The amplitude of the velocity profile of nanoliquid decreases when the Ha number increases, and the maximum value of the velocity profile decreases almost 74.43% when the Hartmann number increases from 0 to 90. This is due to the improvement of the term source term described in Eqs (2) and (3). In this zone, the electromagnetic force is dominant.

In the second zone $(0.33 < X < 0.55)$, the velocity profile is equal to zero due to the presence of the obstacle in the middle of the channel. In the third zone $(0.55 \leq X \leq 0.61)$, a recirculation zone is obtained, and behind the heat source, we can detect that the amplitude of the velocity profile increases. The maximum value of the velocity profile increases about 20% when the Hartmann number increases from 0 to 90. In this zone, the viscous force is dominant. For the last zone $(0.61 < X \leq 1)$, the amplitude of velocity profile decreases with an increasing Ha; at the same time, the horizontal velocity profile increases. The maximum value of the velocity profile decreases almost 89.57% when the Hartmann number increases from 0 to 90. This can be explained by the domination of the conduction heat transfer mode and the effect of Lorentz force. Fig. 11 (c) describes the variation of the temperature profiles along the horizontal direction for different Hartmann numbers. This figure shows that for all values of the Hartmann number, the temperature profile of the nanoliquid in the channel increases in the zone behind the heat source. The augmentation of Hartmann number (from 0 to 90) gives a positive effect on the amplitude of the temperature profile. As a result, the enhancement of Hartmann number gives a diminution of the convective heat transfer mode and augmentation of the conductive heat transfer mode.

7.6. Effect of magnetic field inclination angle

Fig. 12 shows the effect of magnetic field inclination angle on the Nuavg (left) and Sgen (right) for Ha=50, Re=150 and $\phi = 0.02$. In Fig. 12 (a), the average Nusselt number varies with different values of γ. Besides, the heat transfer is maximum for $(\gamma = 0, \pi/3, 2\pi/3, \pi)$. The result indicates a diminution in the Nuavg about 5.65% when the magnetic field inclination angle changes from inclination $(\gamma = 0)$ to $(\gamma = \pi/2)$. This can be explained by the existence of magnetic force in the term of volume forces.

Fig. 12 (b) presents the influence of the magnetic field inclination angle on the total entropy generation for Re=100 and 150. The total entropy generation varies with the magnetic field inclination angle (γ). The main responsibility of this evaluation is the increase in the term due to the magnetic field irreversibility. Also, when increasing the angle of inclination $(\gamma = \pi/2)$, the vertical velocity of the flow is increased, and the maximum value of total entropy generation is detected. On the other hand, when the angle of inclination is equal to zero $(\gamma = 0)$, the horizontal velocity is increased, and we can detect the minimum value of the total entropy generation.
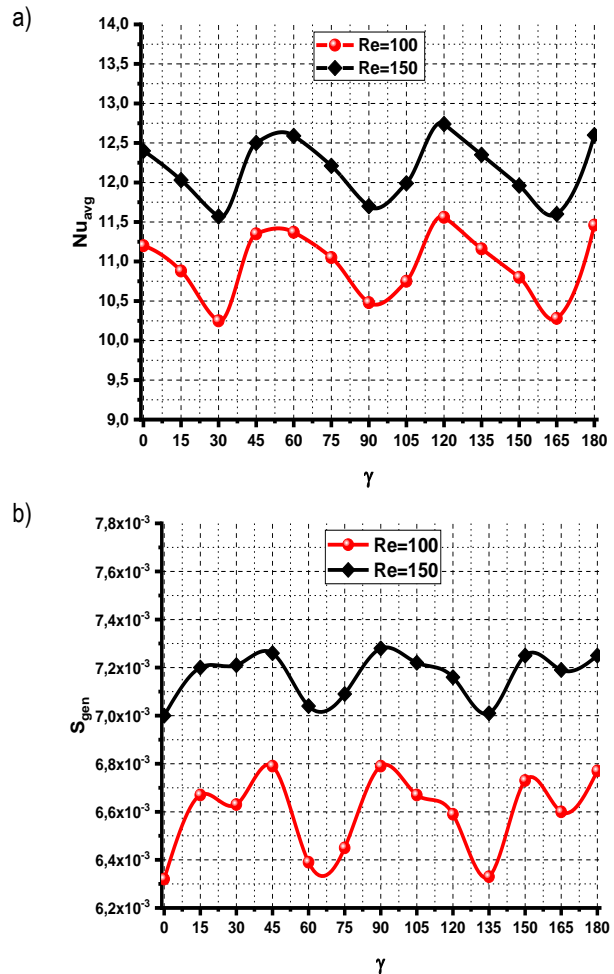

Fig. 12. Variations of the Nuavg(left) and Sgen (right) versus the magnetic inclination angle for Ha = 50, Re = 150 and $\phi = 0.02$

7.7. Effect of Brownian motion

Fig. 13 illustrates the impact of the Brownian motion on the Nuavg (a), Sgen (b) and Be (c) for Re=150, Ha=50 and $\gamma = 0$. The results show that the average Nusselt number is an increasing function of nanoparticle volume fraction. Fig. 13 (a). As ϕ increases, the heat transfer becomes very important for the case with Brownian motion. Besides, this improvement can be explained by the high thermal conductivity of the mixture in the nanoliquid. The heat transfer is enhanced by 10% for the two cases for $1\% \leq \phi \leq 4\%$. The collision between the particles causes an increase in Brownian diffusivity. Therefore, the Brownian motion increases in nanoliquid, which gives an increase in the Nuavg.

Fig. 13 (b) and (c) illustrate the impact of the Brownian motion on the total entropy generation and Bejan number, respectively. The results show that the

The curves in Fig. 13 (b) and (c) shows that the variations of total entropy generation and the curve of the Bejan number are similar to the curve of the average Nusselt number. A great part of the Sgen is due to the increasing heat transfer by the Re increase.
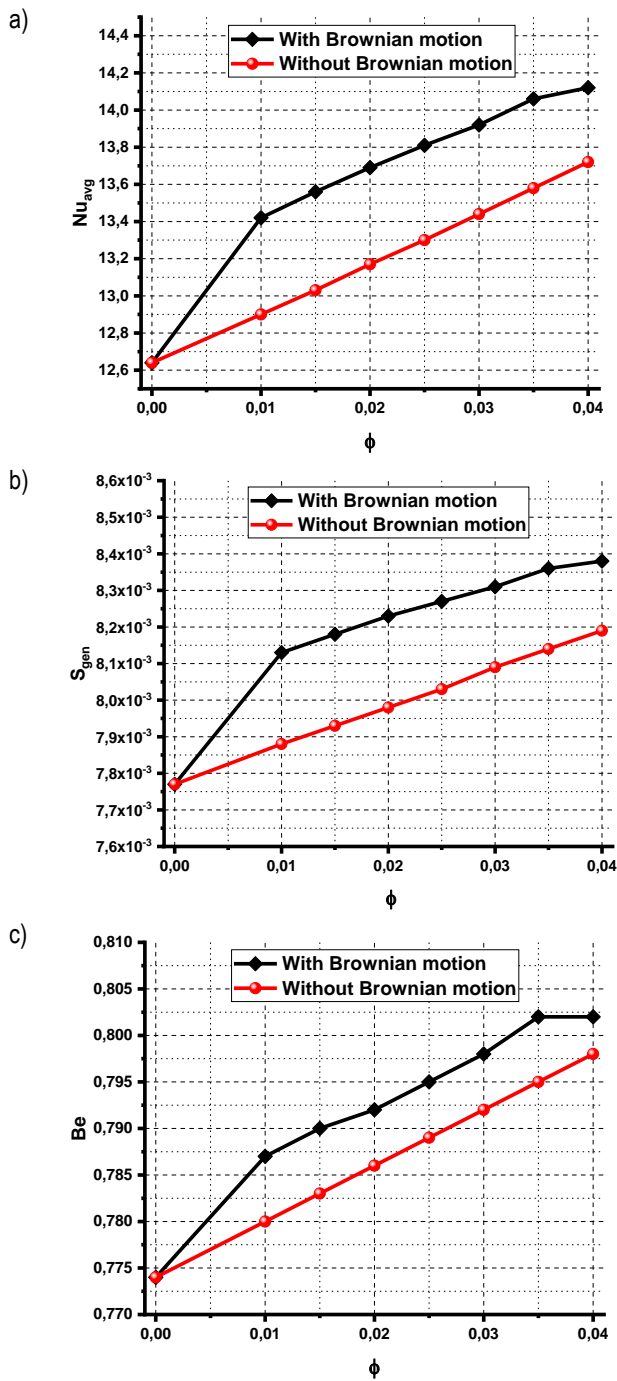
a)

b)

c)

Fig. 13. Impact of Brownian motion on the average Nusselt number (a),
S_{gen} (b) and Be (c) for Re = 150, Ha = 50 and $\gamma = 0$

8. CONCLUSIONS

This numerical study performs MHD forced convection in a channel containing a hot block, flowed with a cold nanoliquid at the inlet and crossed with Cu–water nanoliquid. The LBM is used for resolving the governing equations. The flow characteristics is studied under the effect of several parameters ($0\% \leq \phi \leq 4\%$, 5 nm≤dp≤55 nm, 50≤Re≤200, 0≤Ha≤90, $0 \leq \gamma \leq \pi$) and Brownian motion. We have given particular attention to the impact of several parameters on velocity and temperature profiles after and behind the hot block. The most important findings are concluded as follows:

- The maximum value of the average Nusselt number is found for case (3) when the hot block is placed between the two hot walls. The minimum value of the average Nusselt number is found for case (2) when the hot block is situated between the two insulated walls. Also, the total entropy generation is minimal for case (2) and maximal for case (1).
- Asϕ, Re and Ha increase, the heat transfer, total entropy generation and Bejan number are enhanced.
- As the size of nanoparticles increases, the heat transfer, total entropy generation and Bejan number reduced.
- The recirculation zone is detected behind the hot block for high values of Re numbers (Re=150), and it has an opposite effect to the Reynolds number on the heat transfer.
- The Hartmann number has a positive effect, and the impact of electromagnetic force is detected for$(Ha > 0)$, so the amplitude of vertical velocity increases.
- The magnetic field inclination angle has a very important role to the orientation of the nanoliquid. Consequently, diminution in the Nuavg about 5.65% when the magnetic field inclination angle changes from ($\gamma = 0$) to ($\gamma = \pi/2$).
- The maximum of the total entropy generation is detected with the angle of inclination ($\gamma = \pi/2$), and the minimum value is detected for the angle of inclination ($\gamma = 0$).
- The Be reduces with 41.4% for Re=100, and it reduces about 33.3% for Re= 150 when the Ha increases from 0 to 90.
- The results show that the presence of Brownian motion gives an increasing effect on Nuavg, and the total entropy generation is enhanced by 2.4% for the case with Brownian motion compared to the case without Brownian motion.

REFERENCES

1. Karimipour A, Nezhad AH, D'Orazio A, Esfe MH, Safaei MR, Shirani E. Simulation of copper–water nanofluid in a microchannel in slip flow regime using the lattice Boltzmann method. European Journal of Mechanics-B/Fluids. 2015; 49(A):89-99.
2. Sheikholeslami M, Ashorynejad H, Rana P. Lattice Boltzmann simulation of nanofluid heat transfer enhancement and entropy generation. Journal of Molecular Liquids. 2016; 214:86-95.
3. Mishra P, Tiwari A, Chhabra R. Effect of orientation on forced convection heat transfer from a heated cone in Bingham plastic fluids. International Communications in Heat and Mass Transfer. 2018; 93:34-40.
4. Kim SK. Forced convection heat transfer for the fully-developed laminar flow of the cross fluid between parallel plates. Journal of Non-Newtonian Fluid Mechanics. 2020; 276:104226-1042231.
5. Peyghambarzadeh S, Sarafraz MM, Vaeli N, Ameri E, Vatani A, Jamialahmadi M. Forced convective and subcooled flow boiling heat transfer to pure water and n-heptane in an annular heat exchanger. Annals of Nuclear Energy. 2013; 53:401-410.
6. Arasteh H, Mashayekhi R, Goodarzi M, Motaharpour SH, Dahari M, Toghraie D. Heat and fluid flow analysis of metal foam embedded in a double-layered sinusoidal heat sink under local thermal non-equilibrium condition using nanofluid. Journal of Thermal Analysis and Calorimetry. 2019; 138(2):1461-1476.
7. Farooq U, Waqas H, Khan MI, Khan SU, Chu Y-M, Kadry S. Thermally radioactive bioconvection flow of Carreau nanofluid with modified Cattaneo-Christov expressions and exponential space-based heat source. Alexandria Engineering Journal. 2021; 60(3):3073-3086.
8. Xiong P-Y, Hamid A, Chu Y-M, Khan MI, Gowda R, Kumar RN, et al. Dynamics of multiple solutions of Darcy–Forchheimer saturated flow of Cross nanofluid by a vertical thin needle point. The European Physical Journal Plus. 2021; 136(3):1-22.

9. Santra AK, Sen S, Chakraborty N. Study of heat transfer due to laminar flow of copper–water nanofluid through two isothermally heated parallel plates. International journal of thermal sciences. 2009; 48(2):391-400.

10. Heidary H, Kermani M. Effect of nano-particles on forced convection in sinusoidal-wall channel. International Communications in Heat and Mass Transfer. 2010; 37(10):1520-1527.

11. Minakov A, Lobasov A, Guzei D, Pryazhnikov M, Rudyak VY. The experimental and theoretical study of laminar forced convection of nanofluids in the round channel. Applied Thermal Engineering. 2015; 88:140-148.

12. Ma Y, Mohebbi R, Rashidi M, Yang Z. Study of nanofluid forced convection heat transfer in a bent channel by means of lattice Boltzmann method. Physics of Fluids. 2018; 30(3):032001.

13. Ramin M, Erfan K, Omid A. A, Davood T, Mehdi B, Milad G. CFD analysis of thermal and hydrodynamic characteristics of hybrid nanofluid in a new designed sinusoidal double-layered microchannel heat sink. Journal of Thermal Analysis and Calorimetry 2018; 134(3):2305–2315.

14. Mohebbi R, Lakzayi H, Sidik NAC, Japar WMAA. Lattice Boltzmann method based study of the heat transfer augmentation associated with Cu/water nanofluid in a channel with surface mounted blocks. International Journal of Heat and Mass Transfer. 2018; 117:425-435.

15. Lotfi R, Saboohi Y, Rashidi A. Numerical study of forced convective heat transfer of nanofluids: comparison of different approaches. International Communications in Heat and Mass Transfer. 2010; 37(1):74-78.

16. Mahian O, Kolsi L, Amani M, Estellé P, Ahmadi G, Kleinstreuer C, et al. Recent advances in modeling and simulation of nanofluid flows-Part I: Fundamentals and theory. Physics reports. 2019; 790:1-48.

17. Almohammadi H, Vatan SN, Esmaeilzadeh E, Motezaker A, Nokhosteen A. Experimental investigation of convective heat transfer and pressure drop of Al_2O_3/water nanofluid in laminar flow regime inside a circular tube. International Journal of Mechanical and Mechatronics Engineering. 2012; 6(8):1750-1755.

18. Heris SZ, Etemad SG, Esfahany MN. Experimental investigation of oxide nanofluids laminar flow convective heat transfer. International communications in heat and mass transfer. 2006; 33(4):529-535.

19. Ruhani B, Toghraie D, Hekmatifar M, Hadian M. Statistical investigation for developing a new model for rheological behavior of ZnO–Ag (50%–50%)/ Water hybrid Newtonian nanofluid using experimental data. Physica A: Statistical Mechanics and its Applications. 2019; 525:741-751.

20. Abbasi A, Farooq W, Tag-ElDin ESM, Khan SU, Khan MI, Guedri K, et al. Heat transport exploration for hybrid nanoparticle (Cu, Fe3O4) based blood flow via tapered complex wavy curved channel with slip features. Micromachines. 2022; 13(9):1415-1430.

21. Mehrez Z, El Cafsi A.Forced convection magneto-hydrodynamic Al_2O_3–Cu/water hybrid nanofluid flow over a backward-facing step. Journal of Thermal Analysis and Calorimetry. 2019; 135(2): 1417-1427.

22. Hussain S, Ahmed SE. Unsteady MHD forced convection over a backward facing step including a rotating cylinder utilizing Fe3O4-water ferrofluid. Journal of Magnetism and Magnetic Materials. 2019; 484:356-366.

23. Khan MI, Kiyani M, Malik M, Yasmeen T, Khan MWA, Abbas T. Numerical investigation of magnetohydrodynamic stagnation point flow with variable properties. Alexandria Engineering Journal. 2016; 55(3):2367-2673.

24. Chu Y-M, Khan MI, Khan NB, Kadry S, Khan SU, Tlili I, et al. Significance of activation energy, bio-convection and magnetohydrodynamic in flow of third grade fluid (non-Newtonian) towards stretched surface: A Buongiorno model analysis. International Communications in Heat and Mass Transfer. 2020; 118:104893.

25. Peng X, Peterson G. Convective heat transfer and flow friction for water flow in microchannel structures. International journal of heat and mass transfer. 1996; 39(12):2599-2608.

26. Toghraie D, Mashayekhi R, Arasteh H, Sheykhi S, Niknejadi M, Chamkha AJ. Two-phase investigation of water-Al_2O_3 nanofluid in a micro concentric annulus under non-uniform heat flux boundary conditions. International Journal of Numerical Methods for Heat and Fluid Flow. 2019; 30(4):1759-1814.

27. Moraveji A, Toghraie D. Computational fluid dynamics simulation of heat transfer and fluid flow characteristics in a vortex tube by considering the various parameters. International Journal of Heat and Mass Transfer. 2017; 113:432-443.

28. Togun H. Laminar CuO–water nano-fluid flow and heat transfer in a backward-facing step with and without obstacle. Applied Nanoscience. 2016; 6(3):371-378.

29. Alamyane AA, Mohamad AA. Simulation of forced convection in a channel with extended surfaces by the lattice Boltzmann method. Computers and Mathematics with Applications. 2010; 59(7):2421-2451.

30. Anas RQ, Mussa MA. Maximization of heat transfer density from a single-row cross-flow heat exchanger with wing-shaped tubes using constructal design. Heat Transfer. 2021; 50(6):5906-5924.

31. Yang M-H, Yeh R-H, Hwang J-J. Forced convective cooling of a fin in a channel. Energy Conversion and Management. 2010; 51(6):1277-1286.

32. Maia CRM, Aparecido JB, Milanez LF. Heat transfer in laminar flow of non-Newtonian fluids in ducts of elliptical section. International Journal of Thermal Sciences. 2006; 45(11):1066-1072.

33. Khodabandeh E, Rozati SA, Joshaghani M, Akbari OA, Akbari S, Toghraie D. Thermal performance improvement in water nanofluid/GNP–SDBS in novel design of double-layer microchannel heat sink with sinusoidal cavities and rectangular ribs. Journal of Thermal Analysis and Calorimetry. 2019; 136(3):1333-1345.

34. Fanambinantsoa HV, Rakotomanga FdA, Randriaza-namparany MA. Étude numérique de la convection forcée dans un canal rectangulaire horizontal muni d'une protubérance sinusoïdale. Afrique Scince. 2016; 12(6):353-364.

35. Buyruk E, Karabulut K. Enhancement of heat transfer for plate fin heat exchangers considering the effects of fin arrangements. Heat Transfer Engineering. 2018; 39 (15): 1392-1404.

36. Dixit A, Patil AK. Heat transfer characteristics of grooved fin under forced convection. Heat Transfer Engineering. 2015; 36(16): 1409-1416.

37. Ferhi M, Djebali R. Heat Transfer Appraising and Second Law Analysis of Cu-Water Nanoliquid Filled Microchannel: Slip Flow Regime. Romanian Journal of Physics. 2022; 67:605-630.

38. Mejri I, Mahmoudi A, Abbassi MA, Omri A. Magnetic field effect on entropy generation in a nanofluid-filled enclosure with sinusoidal heating on both side walls. Powder Technology.2014; 266:340-353.

39. Atashafrooz M, Sheikholeslami M, Sajjadi H, Delouei AA. Interaction effects of an inclined magnetic field and nanofluid on forced convection heat transfer and flow irreversibility in a duct with an abrupt contraction. Journal of Magnetism and Magnetic Materials. 2019; 478:216-226.

40. Ferhi M, Djebali R, Mebarek-Oudina F, Abu-Hamdeh NH, Abboudi S. Magnetohydrodynamic Free Convection Through Entropy Generation Scrutiny of Eco-Friendly Nanoliquid in a Divided L-Shaped Heat Exchanger with Lattice Boltzmann Method Simulation. Journal of Nanofluids.2022; 11(1):99-112.

41. Djebali R, Jaouabi A, Naffouti T, Abboudi S. Accurate LBM appraising of pin-fins heat dissipation performance and entropy generation in enclosures as application to power electronic cooling. International Journal of Numerical Methods for Heat and Fluid Flow. 2019; 30(2):742-768.

42. Zou Q, He X. On pressure and velocity boundary conditions for the lattice Boltzmann BGK model. Physics of fluids. 1997; 9(6):1591-1598.

43. Mohamad A. Lattice Boltzmann Method: Fundamentals and Engineering Applications with Computer Codes: Springer Science and Business Media; 2011:70.

44. Brinkman HC. The viscosity of concentrated suspensions and solutions. The Journal of chemical physics. 1952; 20(4):571-579.

45. Koo J, Kleinstreuer C. Laminar nanofluid flow in microheat-sinks. International journal of heat and mass transfer. 2005; 48(13):2652-2661.

46. Hussain S, Ahmed SE, Akbar T. Entropy generation analysis in MHD mixed convection of hybrid nanofluid in an open cavity with a horizontal channel containing an adiabatic obstacle. International Journal of Heat and Mass Transfer. 2017; 114:1054-1066.

47. Tang G, Tao W, He Y. Simulation of fluid flow and heat transfer in a plane channel using the lattice Boltzmann method. International journal of modern physics B. 2003; 17(1):183-187.

48. Izadi M, Mohebbi R, Karimi D, Sheremet MA. Numerical simulation of natural convection heat transfer inside a ⊥ shaped cavity filled by a MWCNT-Fe3O4/water hybrid nanofluids using LBM. Chemical Engineering and Processing-Process Intensification. 2018; 125:56-66.

Rached Miri: https://orcid.org/0000-0001-9113-5370

Mohamed A. Abbassi: https://orcid.org/0000-0002-1915-0944

Mokhtar Ferhi: https://orcid.org/0000-0002-6677-3335

Ridha Djebali: https://orcid.org/0000-0002-1017-3410